



UNIVERSITAT POLITÈCNICA DE CATALUNYA  
BARCELONATECH

Escola Superior d'Enginyeries Industrial,  
Aeroespacial i Audiovisual de Terrassa

# Interplanetary trajectories Patched Conic Approximation (PCA)

---

## Report

**Degree:** Master's degree in Aerospace Engineering

**Course:** 220301 - Aerodynamics, Flight and Orbital Mechanics

**Delivery date:** 15-01-2018

**Students:** Fontanes Molina, Pol; Martínez Viol, Víctor; Urbano González, Eva María



# Contents

|  |            |
|--|------------|
| <b>List of Tables</b>  | <b>ii</b>  |
| <b>List of Figures</b>   | <b>iii</b> |
| <b>1 Aim</b>   | <b>1</b>   |
| <b>2 Theoretical background</b>  | <b>2</b>   |
| 2.1 Planetary orbits and approximations analysis . . . . .                     | 2          |
| 2.1.1 Patched Conic Approximation (PCA) . . . . .                              | 2          |
| 2.1.1.1 1st. Geocentric stage . . . . .  | 3          |
| 2.1.1.2 2nd. Heliocentric stage . . . . .                                      | 6          |
| 2.1.1.3 3rd. Planetocentric stage . . . . .                                    | 12         |
| <b>3 Calculations and results</b>  | <b>13</b>  |
| 3.1 Verification . . . . .   | 13         |
| 3.1.1 From Earth to Mars using an elliptic heliocentric trajectory . . . . .   | 13         |
| 3.1.2 From Mars to Jupiter using an elliptic heliocentric trajectory . . . . . | 14         |
| 3.1.3 From Earth to Mars using an hyperbolic heliocentric trajectory . . . . . | 15         |
| 3.1.4 Verification conclusions . . . . .                                       | 16         |
| 3.2 Main interplanetary orbit calculations . . . . .                           | 16         |
| 3.2.1 Case 1: Mars to Jupiter . . . . .  | 17         |
| 3.2.2 Case 2: Earth to Mars . . . . .  | 17         |
| 3.2.3 Case 3: Earth to Mars . . . . .  | 18         |
| 3.2.4 Case 4: Earth to Mars . . . . .  | 18         |
| 3.2.5 Case 5: Earth to Venus . . . . .   | 19         |
| 3.2.6 Case 6: Mars to Earth . . . . .  | 19         |
| 3.2.7 Case 7: Mars to Earth . . . . .  | 20         |
| 3.2.8 Case 8: Earth to Mars (hyperbolic) . . . . .                             | 20         |
| 3.2.9 Case 9: Earth to Mars (hyperbolic) . . . . .                             | 21         |
| <b>4 Conclusions</b>   | <b>22</b>  |
| <b>5 Bibliography</b>  | <b>23</b>  |

# List of Tables

|        |   |    |
|--------|---|----|
| 2.1.1  | Radius of influence of the planets . . . . .                            | 3  |
| 3.1.1  | Data provided by the first example . . . . .                            | 13 |
| 3.1.2  | Results provided by the first example . . . . .                         | 13 |
| 3.1.3  | Results computed by the code developed for the first example . . . . .  | 14 |
| 3.1.4  | Relative error in the first example . . . . .                           | 14 |
| 3.1.5  | Data provided by the second example . . . . .                           | 14 |
| 3.1.6  | Results provided by the second example . . . . .                        | 14 |
| 3.1.7  | Results computed by the code developed for the second example . . . . . | 15 |
| 3.1.8  | Relative error in the second example . . . . .                          | 15 |
| 3.1.9  | Data provided by the third example . . . . .                            | 15 |
| 3.1.10 | Results provided by the third example . . . . .                         | 15 |
| 3.1.11 | Results computed by the code developed for the third example . . . . .  | 16 |
| 3.1.12 | Relative error in the third example . . . . .                           | 16 |
| 3.2.1  | Data provided for a travel between Mars and Jupiter . . . . .           | 17 |
| 3.2.2  | Results computed for a travel between Mars and Jupiter . . . . .        | 17 |
| 3.2.3  | Data provided for case 2 . . . . .                                      | 17 |
| 3.2.4  | Results computed for case 2 . . . . .                                   | 17 |
| 3.2.5  | Data provided for case 3 . . . . .                                      | 18 |
| 3.2.6  | Results computed for case 3 . . . . .                                   | 18 |
| 3.2.7  | Data provided for case 4 . . . . .                                      | 18 |
| 3.2.8  | Results computed for case 4 . . . . .                                   | 18 |
| 3.2.9  | Data provided for case 5 . . . . .                                      | 19 |
| 3.2.10 | Results computed for case 5 . . . . .                                   | 19 |
| 3.2.11 | Data provided for case 6 . . . . .                                      | 19 |
| 3.2.12 | Results computed for case 6 . . . . .                                   | 19 |
| 3.2.13 | Data provided for case 7 . . . . .                                      | 20 |
| 3.2.14 | Results computed for case 7 . . . . .                                   | 20 |
| 3.2.15 | Data provided for case 8 . . . . .                                      | 20 |
| 3.2.16 | Results computed for case 8 . . . . .                                   | 20 |
| 3.2.17 | Data provided for case 9 . . . . .                                      | 21 |
| 3.2.18 | Results computed for case 9 . . . . .                                   | 21 |

List of Figures

2.1.1    Hyperbola Parameters. Extracted from [3]. . . . . 4

2.1.2    Velocities frames of reference. Extracted from [1] . . . . . 5

2.1.3    Injection points circle. Extracted from [1] . . . . . 6

2.1.4    Flow chart for the elliptic trajectory resolution. . . . . 9

2.1.5    Flow chart for the hyperbolic trajectory resolution. . . . . 10

2.1.6    ECI-*IJK* system, extracted from [1]. . . . . 11

# 1 | Aim

This project aims to compute an interplanetary trajectory which, for a given ecliptic rectangular positions of two planets in two known time instances, is able to carry a spaceship with a unique impulse, from the first planet to the second.

## 2 | Theoretical background

### 2.1 Planetary orbits and approximations analysis

In order to calculate the interplanetary trajectory between two planets, several approximations can be used. The simplest approximation, which can be called *aprox. 0* accepts the following hypothesis:

- Circular and coplanar orbits
- No analysis about the exit of the planet of start is done.
- No analysis about entering the planet of arrival is done.

*Aprox. 0* is very basic and can be easily improved adding some parameters.

Another approximation widely used is **Patched Conic Approximation (PCA)**. This method improves significantly the results obtained with *aprox. 0* and represents a good starting point for a more precise numerical analysis of the mission. For this reason, in this project the PCA method will be used.

#### 2.1.1 Patched Conic Approximation (PCA)

The Patched Conic Approximation (PCA) consist on the evaluation of an interplanetary trajectory dividing it into three stages. Considering the Earth as the planet of start, this stages are:

- Geocentric phase: Hyperbolic exit of the Earth. This phase takes place while the probe is going through the influence sphere of the Earth.
- Heliocentric phase: Trajectory with the Sun as main influencer.

## Planetary orbits and approximations analysis

---

- Planet-centred phase: Hyperbolic arrival to the planet of destination. Similarly to the geocentric phase, this phase starts when the probe enters the sphere of influence of the planet.

The influence spheres mentioned are the space close to the planets where it can be considered that the influence of the Sun is negligible in comparison with that of the planet in question. The Laplace criteria will be considered to calculate this sphere. In Table 2.1.1 the radius of the sphere of influence of the solar system's planets are shown.

| Planet  | $R_I \times 10^6 \text{ km}$ | $R_I \times 10^{-3} \text{ UA}$ | $R_I$ Radius of the planet |
|---------|------------------------------|---------------------------------|----------------------------|
| Mercury | 0.111                        | 0.740                           | 45                         |
| Venus   | 0.616                        | 4.11                            | 100                        |
| Earth   | 0.924                        | 6.16                            | 145                        |
| Mars    | 0.577                        | 3.85                            | 170                        |
| Jupiter | 48.157                       | 321.0                           | 677                        |
| Saturn  | 54.796                       | 365.3                           | 901                        |
| Uranus  | 91.954                       | 346.4                           | 2025                       |
| Neptune | 80.196                       | 534.6                           | 3866                       |

Table 2.1.1: Radius of influence of the planets

In order to set out the problem and begin with the resolution of it using the PCA method, the times and positions of the planets at the beginning and end of the trajectory are needed and some hypothesis are taken under consideration. The hypothesis are:

- The spheres of influences of the planets are not considered during the heliocentric phase. This hypothesis is admissible because the radius of the sphere are very small in comparison with the distance between planets.
- The spheres of influence are considered infinite from the point of view of the planet. This is assumed due to the fact that the radius of influence of the planets are much larger than the radius of the planet itself, as can be seen in Tabl 2.1.1.
- The duration of the trajectory can be taken as the duration of the heliocentric phase.

With this data the trajectory can be found through the orbital elements of the trajectories and the thrust required.

### 2.1.1.1 1st. Geocentric stage

This first stage of the trajectory of the probe aims to escape the gravitational field exerted by the departure planet. To achieve this, it is necessary to follow a hyperbolic trajectory that



guarantees to pass through the planet sphere of influence with a relative velocity  $V_\infty$  (also known as hyperbolic excess velocity).

Therefore, in this section necessary equations to characterize this hyperbola will be reviewed. Figure 2.1.1 shows the aforementioned situation. From the figure, it can be inferred that the hyperbola is defined by:

- $C$ : Center of the hyperbola.
- $\beta$ : Angle of the hyperbola.
- $b$ : Exit parameter.

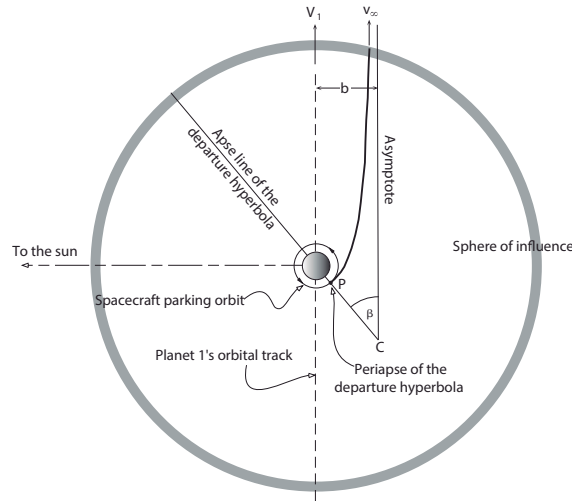


Figure 2.1.1: Hyperbola Parameters. Extracted from [3].

The hyperbola can also be defined by the semi-major axis ( $a$ ) and the eccentricity ( $e$ ). In addition, the  $\Delta V$  necessary to inject the probe into the hyperbolic orbit from the parking orbit must be specified.

To obtain these parameters, only the heliocentric departure speed ( $v_1$ ), the velocity of the departure planet ( $v_p$ ) and the parking orbit (in particular, the periapse radius and the speed of the orbit) are needed.

**Definition of hyperbola:** The first step is to obtain the semi-major axis of the hyperbola. This is obtained from the hyperbolic excess velocity as:

$$a = \frac{\mu}{V_\infty^2} \quad (2.1.1)$$

where  $\mu$  is the standard gravitational parameter ( $\mu = GM$ ) for the sun and the excess velocity is computed as the difference between the probe velocity and the departure planet speed. The eccentricity of hyperbola is defined by:

$$e = 1 + \left(\frac{V_\infty}{V_0}\right)^2 \quad (2.1.2)$$

where  $V_0$  refers to the speed of the parking orbit. If this orbit is assumed to be circular with  $r_0$  as the periaipse, the probe velocity through the parking orbit is given by:

$$V_0 = \sqrt{\mu_0/r_0} \quad (2.1.3)$$

being  $\mu_0$  the standard gravitational parameter of the departure planet. Once the eccentricity is computed, the beta angle is easily obtained as:

$$\cos \beta = \frac{1}{e} \quad (2.1.4)$$

Finally, the exit parameter is computed by means of:

$$b = a\sqrt{e^2 - 1} \quad (2.1.5)$$

Obtaining the center of the hyperbola is a little bit more cumbersome. Given the three velocities ( $V_\infty$ ,  $v_p$  and  $v_1$ ), the two frames of the figure 2.1.2 can be defined. One has the Y-axis in the direction of the planet velocity and the other has the vernal point over the X-axis. Then, the angle between the planet velocity and this X-axis is defined as  $\lambda_v = 90 + \lambda_x$ . Determining this  $\lambda_x$  at the injection time  $t_1$  allows us to obtain the right ascension ( $\alpha$ ) and the declination ( $\delta$ ) of the  $v_1$  velocity by means of a change of frame:

$$\left[V_\infty\right]_{\mathcal{Q}} = \mathcal{R}_1(-\varepsilon)\mathcal{R}_3(-\lambda_x) \left[V_\infty\right]_{\mathcal{K}} \quad (2.1.6)$$

Thus,

$$\sin \delta = [V_z]_{\mathcal{Q}}; \quad \tan \alpha = \left[\frac{V_y}{V_x}\right]_{\mathcal{Q}} \quad (2.1.7)$$

Finally, the center of the hyperbola has the following coordinates  $(\alpha + 12^h, \delta)$ .

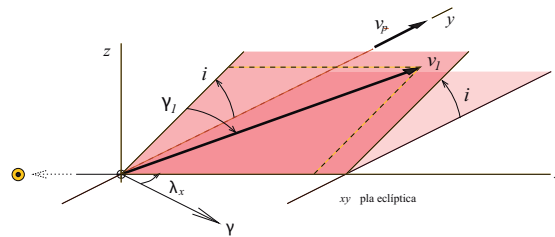


Figure 2.1.2: Velocities frames of reference. Extracted from [1]



**Longitude, latitude and distance** The position vector is defined as:

$$\vec{r} = (x_k, y_k, z_k) \quad (2.1.9)$$

Where:

$$x_k = r \cos \beta \cos \lambda \quad (2.1.10)$$

$$y_k = r \cos \beta \sin \lambda \quad (2.1.11)$$

$$z_k = r \sin \beta \quad (2.1.12)$$

Then longitude, latitude and distance are computed with:

$$r = |\vec{r}| \quad (2.1.13)$$

$$\beta = \arcsin\left(\frac{z_k}{r}\right) \quad (2.1.14)$$

$$\lambda = \arctan\left(\frac{y_k}{x_k}\right) \quad (2.1.15)$$

The difference between  $\lambda$  at the beginning and at the end of the trajectory is an important magnitude that will be used. Taking into account that subscript 1 refers to the start position and subscript 2 to the end:

$$\Delta\lambda = \lambda_2 - \lambda_1 \quad (2.1.16)$$

### **Inclination, right ascension of the ascending node and true anomaly variation**

Trigonometry has to be used to compute this elements. A general case will be considered, that is to say, that no assumption will be done on whether the two planets are on the ecliptic or not. As shown in reference [1], the equations to be used are:

$$\cos \Delta\theta = \sin \beta_1 \sin \beta_2 + \cos \beta_1 \cos \beta_2 \cos \Delta\lambda \quad (2.1.17)$$

$$\sin A = \cos \beta_2 \frac{\sin \Delta\lambda}{\sin \Delta\theta} \quad (2.1.18)$$

$$\cos i = \sin A \cos \beta_1 \quad (2.1.19)$$

$$\sin l = \frac{\tan \beta_1}{\tan i} \quad (2.1.20)$$

$$\tan \sigma = \frac{\tan \beta_1}{\cos A} \quad (2.1.21)$$

$$\Omega = \lambda_1 - l \quad (2.1.22)$$

**Eccentricity, semimajor axis and true anomaly of the starting point** With the aim of obtaining this data three equations can be stated. Due to the complexity of the equations, the resolution will be done iteratively. Two cases will be considered: elliptic and hyperbolic. Its equations and iteration process are now shown:

- Elliptic trajectory: The equations of the elliptic trajectory are:

$$e = \frac{r_2 - r_1}{r_1 \cos \theta_1 - r_2 \cos(\theta_1 + \Delta\theta)} \quad (2.1.23)$$

$$a = \frac{r_1 (1 + e \cos \theta_1)}{1 - e^2} \quad (2.1.24)$$

$$t_2 - t_1 = \frac{365.25}{2\pi} a^{\frac{3}{2}} \left( 2 \arctan \left( \sqrt{\frac{1-e}{1+e}} \tan \frac{\theta_1 + \Delta\theta}{2} \right) - \frac{e \sqrt{1-e^2} \sin(\theta_1 + \Delta\theta)}{1 + e \cos(\theta_1 + \Delta\theta)} - 2 \arctan \left( \sqrt{\frac{1-e}{1+e}} \tan \frac{\theta_1}{2} \right) + \frac{e \sqrt{1-e^2} \sin \theta_1}{1 + e \cos \theta_1} \right) \quad (2.1.25)$$

The iteration process done to solve the equations will deal with the difference between the time of the mission calculated and the real time of the mission, that is a known value. An error criteria  $\epsilon$  is defined as the convergence value. Since the convergence criteria gives a difference in terms of time and the tuning parameter is an angle, there is no possibility to develop an adaptive increase step for  $\theta_1$  (due to their completely different physical meaning). However, a kind of *intelligent* convergence can be applied involving the sign of the time difference multiplying the  $\theta$  step by the time error and dividing it by the time error absolute value.

Another issue related to the algorithm based on tuning an angle is the possibility of entering into a loop between two results if the step used is not small enough. To solve this problem, the algorithm includes a procedure to detect this situation and reduce the  $\theta$  step in order to avoid the loop. The flow chart of this iteration (without the details of the aforementioned convergence system) is shown in Figure 2.1.4.

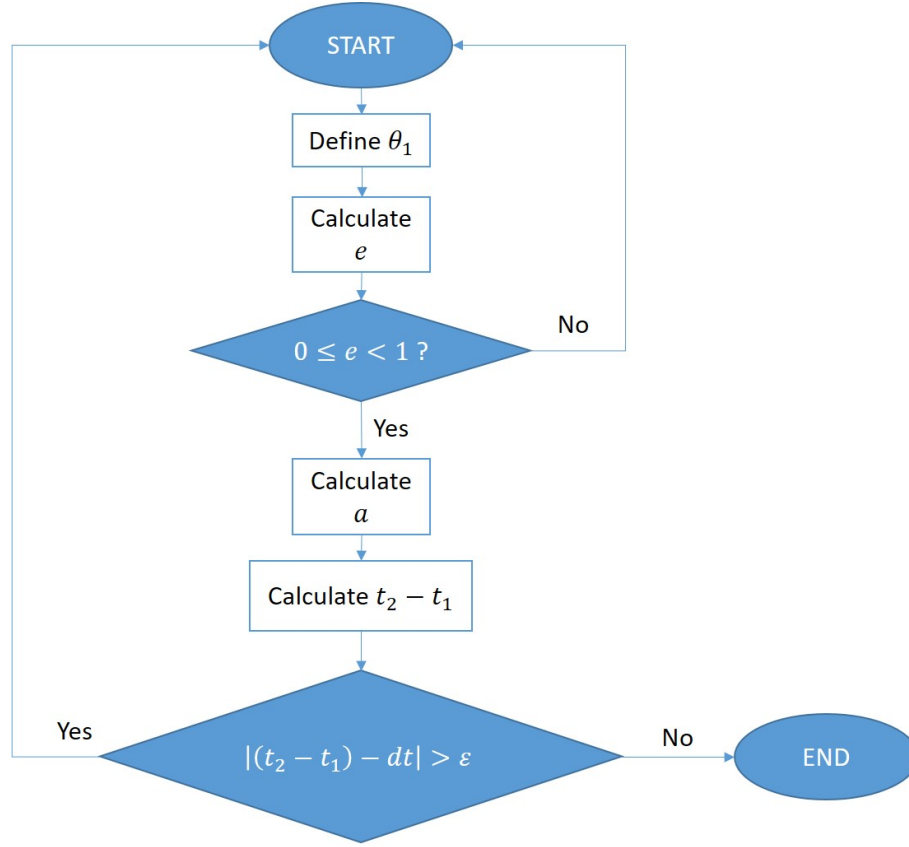


Figure 2.1.4: Flow chart for the elliptic trajectory resolution.

- Hyperbolic trajectory: The equations of the hyperbolic trajectory are:

$$e = \frac{r_2 - r_1}{r_1 \cos \theta_1 - r_2 \cos(\theta_1 + \Delta\theta)} \quad (2.1.26)$$

$$a = \frac{r_1 (1 + e \cos \theta_1)}{e^2 - 1} \quad (2.1.27)$$

$$t_2 - t_1 = \frac{365.25}{2\pi} a^{\frac{3}{2}} \left( \frac{e\sqrt{e^2 - 1} \sin(\theta_1 + \Delta\theta)}{1 + e \cos(\theta_1 + \Delta\theta)} - \ln \left| \frac{\tan \frac{\theta_1 + \Delta\theta}{2} + \sqrt{\frac{e+1}{e-1}}}{\tan \frac{\theta_1 + \Delta\theta}{2} - \sqrt{\frac{e+1}{e-1}}} \right| - \frac{e\sqrt{e^2 - 1} \sin \theta_1}{1 + e \cos \theta_1} + \ln \left| \frac{\tan \frac{\theta_1}{2} + \sqrt{\frac{e+1}{e-1}}}{\tan \frac{\theta_1}{2} - \sqrt{\frac{e+1}{e-1}}} \right| \right) \quad (2.1.28)$$

The resolution is similar to that of the elliptic case, but the acceptable values of the eccentricity change. The flow chart is shown in Figure 2.1.5.

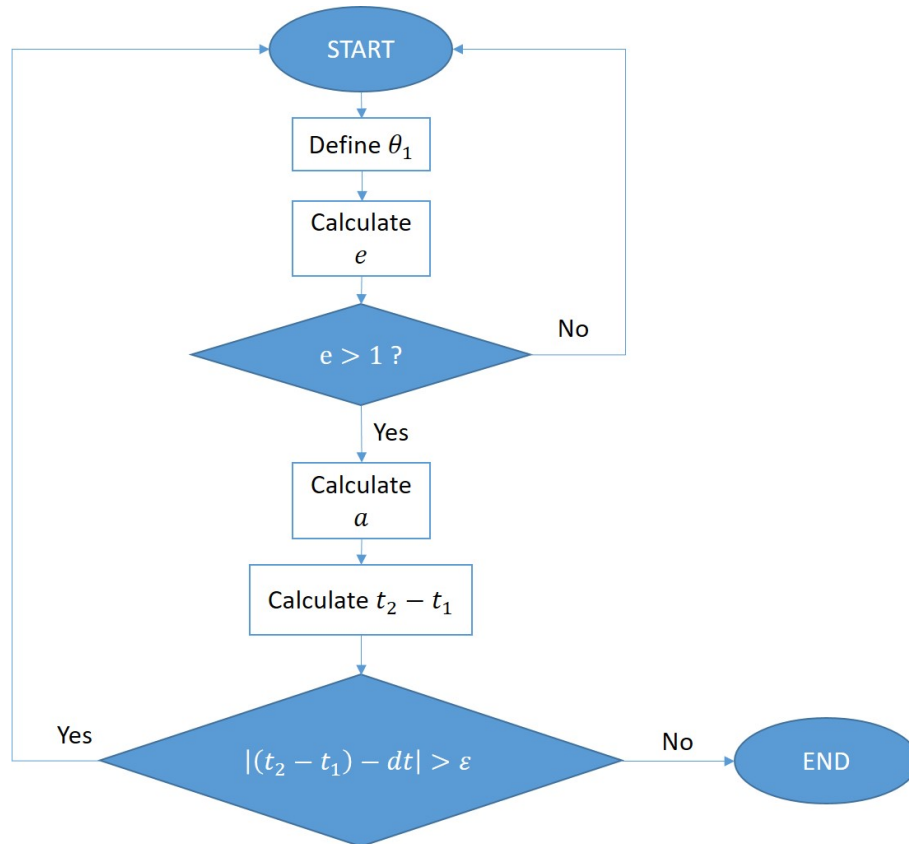


Figure 2.1.5: Flow chart for the hyperbolic trajectory resolution.

**Argument of the perihelion** The only remaining orbit element that needs to be computed is  $\omega$ . It can be calculated using results from the previous steps:

$$\omega = 2\pi - (\theta_1 - \sigma) \quad (2.1.29)$$

**Spacecraft velocity** Sphere Of Influence (SOI), departure and arrival velocities are computed under the following theoretical background.

First of all, a geocentric coordinates system is considered with the orbital plane  $PQW(\bar{x}, \bar{y}, \bar{z})$ . The spacecraft orbit is situated on the system  $ECI-IJK$ , seen on the following figure.

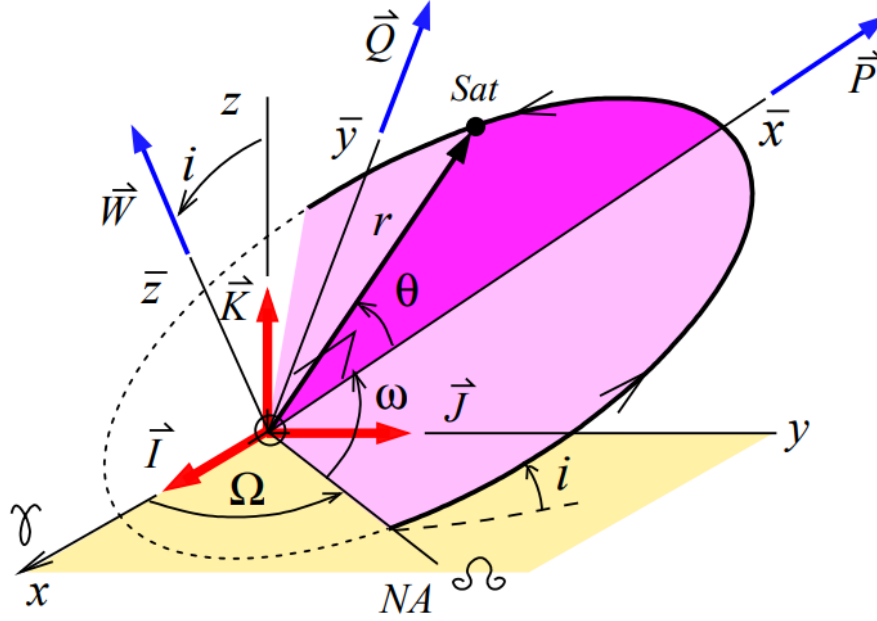


Figure 2.1.6: ECI-*IJK* system, extracted from [1].

A series of rotations are done, for changing from the orbital plane *PQW* to the equatorial *IJK*. A,  $\mathbb{M}$  rotation matrix is defined:

$$\mathbb{M}(\omega, i, \Omega) = \mathbb{R}_3(-\Omega) \cdot \mathbb{R}_3(-i) \cdot \mathbb{R}_3(-\omega)$$

with the following components:

$$\begin{aligned} \mathbb{M}_{11} &= P_x = +\cos \Omega \cos \omega - \sin \Omega \cos i \sin \omega \\ \mathbb{M}_{21} &= P_y = +\sin \Omega \cos \omega + \cos \Omega \cos i \sin \omega \\ \mathbb{M}_{31} &= P_z = \sin i \sin \omega \\ \mathbb{M}_{12} &= Q_x = -\cos \Omega \sin \omega - \sin \Omega \cos i \cos \omega \\ \mathbb{M}_{22} &= Q_y = -\sin \Omega \sin \omega + \cos \Omega \cos i \cos \omega \\ \mathbb{M}_{32} &= Q_z = +\sin i \cos \omega \\ \mathbb{M}_{13} &= W_x = +\sin \Omega \sin i \\ \mathbb{M}_{23} &= W_y = -\cos \Omega \sin i \\ \mathbb{M}_{33} &= W_z = +\cos i \end{aligned} \tag{2.1.30}$$

Therefore, spacecraft geocentric position vector  $\vec{r}$  is:

$$\vec{r} = \bar{x}\vec{P} + \bar{y}\vec{Q} = x\vec{I} + y\vec{J} + z\vec{K} \tag{2.1.31}$$

with

$$\vec{P} = P_X\vec{I} + P_Y\vec{J} + P_Z\vec{K} \tag{2.1.32}$$



Finally, heliocentric  $\vec{r}$  and  $\dot{\vec{r}}$  can be computed using  $\vec{P}$ ,  $\vec{Q}$ ,  $\vec{W}$  unitary vectors, as

$$\vec{r} = r[\cos \theta \cdot \vec{P} + \sin \theta \cdot \vec{Q}] \quad (2.1.33)$$

$$\dot{\vec{r}} = \sqrt{\frac{\mu_{\odot}}{p}}[-\sin \theta \cdot \vec{P} + (e + \cos \theta) \cdot \vec{Q}] \quad (2.1.34)$$

taking into account that parameter  $p$  is  $p = a(1 - e^2)$  for elliptic trajectories and  $p = a(e^2 - 1)$  for hyperbolic ones.

Also for computing  $\vec{r}$  and  $\dot{\vec{r}}$  for the departure and arrival cases,  $\theta$ , the true anomaly is

$$\text{Departing SOI: } \theta = \theta_0 \quad \text{Arriving SOI: } \theta = \theta_1 = \theta_0 + \Delta\theta$$

In conclusion, for calculating the spacecraft heliocentric departure and arrival velocities to the SOI of each planet, previously the heliocentric orbital elements would have to be calculated following the equations exposed before the velocity paragraph. Because, for this study the planets position vectors are given, we can verify the correction of velocity equations  $\dot{\vec{r}}$ , comparing the given position vector with the one calculated,  $\vec{r}$ , they should match.

### 2.1.1.3 3rd. Planetocentric stage

Once the spacecraft, enter into the SOI of the destination planet, the planetocentric stage starts. The spacecraft, describes a planet arrival hyperbola. Depending of the arrival velocity and position three main scenarios can be described for the spacecraft.

**Impact** If arrival position  $r_p \leq R_P$ .

**Slowdown** Atmosphere interaction will slowdown the spacecraft if  $r_p \leq R_a$ .

**Flyby** Spacecraft will perform a flyby over the planet if  $r_p > R_a$  or  $b > b_a$ .

Note that  $R_P$  and  $R_a$ , correspond to the planet and atmosphere radius respectively.

The spacecraft, will only stay trapped on the destination planet, orbiting, if the spaceship has slowdown enough in contact with the planet atmosphere or the spaceship braked during the periastron.

Because, the main assignment objective was to calculate, a trajectory between to planets for interplanetary travel. This stage is been only develop theoretically, expressions for computing theses parameters can be obtained on, [1]. First and third stage of the PCA, share some concepts and equations because in both, an hyperbolic trajectory is performed.

## 3 | Calculations and results

### 3.1 Verification

In order to verify the code the examples shown at reference [2] will be used. In this section the results provided for every example will be exposed together with the results obtained using the code developed for this project and conclusions will be extracted.

#### 3.1.1 From Earth to Mars using an elliptic heliocentric trajectory

|                |                           |
|----------------|---------------------------|
| Departure date | 2020 Jul 19               |
| Arrival date   | 2021 Gen 25               |
| $\Delta t$     | 190 days                  |
| $r_1$          | (0.4537, -0.9094, 0.0000) |
| $r_2$          | (0.3148, 1.5078, 0.0239)  |

Table 3.1.1: Data provided by the first example

|   |                            |
|---|----------------------------|
| Semimajor axis                            | 1.33069 AU                 |
| Eccentricity                              | 0.23629                    |
| $\theta_0$                                | 359.621°                   |
| $\omega$                                  | 0.470°                     |
| Inclination                               | 1.435°                     |
| $\Omega$                                  | 296.424°                   |
| Heliocentric velocity at departure (km/s) | (29.3678, 14.6982, 0.8229) |
| Heliocentric velocity at arrival (km/s)   | (20.4069, 8.2271, 0.3656)  |

Table 3.1.2: Results provided by the first example

|   |                                |
|---|--------------------------------|
| Semimajor axis                            | 1.33073 AU                     |
| Eccentricity                              | 0.236291                       |
| $\theta_0$                                | 359.613°                       |
| $\omega$                                  | 0.386861°                      |
| Inclination                               | 1.43388°                       |
| $\Omega$                                  | 296.515°                       |
| Heliocentric velocity at departure (km/s) | (29.367, 14.6986, 0.822024)    |
| Heliocentric velocity at arrival (km/s)   | (-20.4068, 8.27743, -0.364583) |

Table 3.1.3: Results computed by the code developed for the first example

| Parameter  | Relative error (%) |
|------------|--------------------|
| a          | 0.0030             |
| e          | 0.0004             |
| $\theta_0$ | 0.0022             |
| $\omega$   | 17.6891            |
| i          | 0.0780             |
| $\Omega$   | 0.0307             |
| $v_{t_1}$  | 0.0017             |
| $v_{t_1}$  | 0.0001             |

Table 3.1.4: Relative error in the first example

### 3.1.2 From Mars to Jupiter using an elliptic heliocentric trajectory

|                |                          |
|----------------|--------------------------|
| Departure date | 2026 Jun 05              |
| Arrival date   | 2029 April 25            |
| $\Delta t$     | 1055 days                |
| $r_1$          | (1.3277, 0.4901, 0.0223) |
| $r_2$          | (5.0135, 2.1380, 0.0505) |

Table 3.1.5: Data provided by the second example

|   |                            |
|---|----------------------------|
| Semimajor axis                            | 3.45403 AU                 |
| Eccentricity                              | 0.59218                    |
| $\theta_0$                                | 350.769°                   |
| $\omega$                                  | 182.312°                   |
| Inclination                               | 7.513°                     |
| $\Omega$                                  | 207.121°                   |
| Heliocentric velocity at departure (km/s) | (12.5324, 28.6817, 4.1200) |
| Heliocentric velocity at arrival (km/s)   | (1.9715, 7.9799, 1.0552)   |

Table 3.1.6: Results provided by the second example

|   |                               |
|---|-------------------------------|
| Semimajor axis                            | 3.45405                       |
| Eccentricity                              | 0.592181                      |
| $\theta_0$                                | 350.469°                      |
| $\omega$                                  | 196.156°                      |
| Inclination                               | 7.508444°                     |
| $\Omega$                                  | 207.127°                      |
| Heliocentric velocity at departure (km/s) | (-19.0894, 24.8148, -4.05809) |
| Heliocentric velocity at arrival (km/s)   | (3.83725, -7.26513, 1.08284)  |

Table 3.1.7: Results computed by the code developed for the second example

| Parameter  | Relative error (%) |
|------------|--------------------|
| a          | 0.0006             |
| e          | 0.0002             |
| $\theta_0$ | 0.0000             |
| $\omega$   | 7.5936             |
| i          | 0.0606             |
| $\Omega$   | 0.0029             |
| $v_{t_1}$  | 0.0014             |
| $v_{t_1}$  | 0.0001             |

Table 3.1.8: Relative error in the second example

### 3.1.3 From Earth to Mars using an hyperbolic heliocentric trajectory

|                |                            |
|----------------|----------------------------|
| Departure date | 2020 Mar 06                |
| Arrival date   | 2020 Jun 09                |
| $\Delta t$     | 95 days                    |
| $r_1$          | (-0.9609, 0.2466, 0.0000)  |
| $r_2$          | (0.7285, -1.1980, -0.0430) |

Table 3.1.9: Data provided by the third example

|   |                             |
|---|-----------------------------|
| Semimajor axis                            | 71.08581 AU                 |
| Eccentricity                              | 1.01113                     |
| $\theta_0$                                | -53.310°                    |
| $\omega$                                  | 233.297°                    |
| Inclination                               | 2.513°                      |
| $\Omega$                                  | 345.619°                    |
| Heliocentric velocity at departure (km/s) | (9.1364, -41.4090, -1.6612) |
| Heliocentric velocity at arrival (km/s)   | (35.1754, -6.3201, 0.1148)  |

Table 3.1.10: Results provided by the third example

## Main interplanetary orbit calculations

---

|   |                             |
|---|-----------------------------|
| Semimajor axis                            | 71.6165                     |
| Eccentricity                              | 1.01105                     |
| $\theta_0$                                | 306.691°                    |
| $\omega$                                  | 233.309°                    |
| Inclination                               | 2.51416°                    |
| $\Omega$                                  | 345.607°                    |
| Heliocentric velocity at departure (km/s) | (9.13562,-41.4082,-1.66139) |
| Heliocentric velocity at arrival (km/s)   | (35.1747,-6.31841,0.115199) |

Table 3.1.11: Results computed by the code developed for the third example

| Parameter  | Relative error (%) |
|------------|--------------------|
| a          | 0.7465             |
| e          | 0.0079             |
| $\theta_0$ | 0.0003             |
| $\omega$   | 0.0051             |
| i          | 0.0462             |
| $\Omega$   | 0.0035             |
| $v_{t_1}$  | 0.1189             |
| $v_{t_1}$  | 0.0028             |

Table 3.1.12: Relative error in the third example

### 3.1.4 Verification conclusions

It can be appreciated that in most of the cases the relative error is far less than one. The highest error produced is less than 10%, and its cause probably deal with the equations and assumptions done while computing the results.

The code is taken as valid and can be used in order to obtain other interplanetary trajectory. It has been done in a general manner so the same code can compute elliptic and hyperbolic trajectories with any departure and arrival planet in the solar system.

## 3.2 Main interplanetary orbit calculations

The cases proposed in reference [2] will be solved.

**3.2.1 Case 1: Mars to Jupiter**

|                |                          |
|----------------|--------------------------|
| Departure date | 2037 Oct 25              |
| Arrival date   | 2039 Oct 15              |
| $\Delta t$     | 720 days                 |
| $r_1$          | (1.0707, 0.9868, 0.0055) |
| $r_2$          | (5.2210, 1.4357, 0.1109) |

Table 3.2.1: Data provided for a travel between Mars and Jupiter

|   |                                |
|---|--------------------------------|
| Semimajor axis                            | 4.27012                        |
| Eccentricity                              | 0.725509                       |
| $\theta_0$                                | 302.422 °                      |
| $\omega$                                  | 63.3568°                       |
| Inclination                               | 2.14985°                       |
| $\Omega$                                  | 36.89°                         |
| Heliocentric velocity at departure (km/s) | (-29.1352, 12.6808, 1.03727)   |
| Heliocentric velocity at arrival (km/s)   | (4.72014, -9.86931, -0.402679) |

Table 3.2.2: Results computed for a travel between Mars and Jupiter

**3.2.2 Case 2: Earth to Mars**

|                |                          |
|----------------|--------------------------|
| Departure date | 2033 Mar 13              |
| Arrival date   | 2033 Aug 05              |
| $\Delta t$     | 145 days                 |
| $r_1$          | (0.9848, 0.1338, 0.0000) |
| $r_2$          | (0.6797, 1.2298, 0.0424) |

Table 3.2.3: Data provided for case 2

|   |                                |
|---|--------------------------------|
| Semimajor axis                            | 1.37053                        |
| Eccentricity                              | 0.615632                       |
| $\theta_0$                                | 256.507°                       |
| $\omega$                                  | 103.493°                       |
| Inclination                               | 2.15438°                       |
| $\Omega$                                  | 7.73712°                       |
| Heliocentric velocity at departure (km/s) | (-22.8707, 24.7746, 1.03934)   |
| Heliocentric velocity at arrival (km/s)   | (9.73264, -22.7879, -0.898741) |

Table 3.2.4: Results computed for case 2

### 3.2.3 Case 3: Earth to Mars

|                |                          |
|----------------|--------------------------|
| Departure date | 2031 Jan 23              |
| Arrival date   | 2031 Aug 01              |
| $\Delta t$     | 190 days                 |
| $r_1$          | (0.5264, 0.8316, 0.0001) |
| $r_2$          | (0.0108, 1.4542, 0.0309) |

Table 3.2.5: Data provided for case 3

|   |                              |
|---|------------------------------|
| Semimajor axis                            | 1.24706                      |
| Eccentricity                              | 0.381113                     |
| $\theta_0$                                | 282.584 °                    |
| $\omega$                                  | 77.5612 °                    |
| Inclination                               | 2.29274 °                    |
| $\Omega$                                  | 57.8117 °                    |
| Heliocentric velocity at departure (km/s) | (-48.5598, 30.3938, 2.29362) |
| Heliocentric velocity at arrival (km/s)   | (20.646, -0.03366, -0.70028) |

Table 3.2.6: Results computed for case 3

### 3.2.4 Case 4: Earth to Mars

|                |                          |
|----------------|--------------------------|
| Departure date | 2025 Jul 18              |
| Arrival date   | 2025 Oct 21              |
| $\Delta t$     | 95 days                  |
| $r_1$          | (0.4342, 0.9188, 0.0001) |
| $r_2$          | (0.6775, 1.3571, 0.0118) |

Table 3.2.7: Data provided for case 4

|   |   |
|---|---|
| Semimajor axis                            |   |
| Eccentricity                              |   |
| $\theta_0$                                | ° |
| $\omega$                                  | ° |
| Inclination                               | ° |
| $\Omega$                                  | ° |
| Heliocentric velocity at departure (km/s) |   |
| Heliocentric velocity at arrival (km/s)   |   |

Table 3.2.8: Results computed for case 4

### 3.2.5 Case 5: Earth to Venus

|                |                            |
|----------------|----------------------------|
| Departure date | 2023 May 27                |
| Arrival date   | 2023 Nov 01                |
| $\Delta t$     | 158 days                   |
| $r_1$          | (-0.4255, -0.9194, 0.0000) |
| $r_2$          | (0.0356, 0.7189, 0.0079)   |

Table 3.2.9: Data provided for case 5

|   |                                |
|---|--------------------------------|
| Semimajor axis                            | 217.426                        |
| Eccentricity                              | -0.847689                      |
| $\theta_0$                                | 360.007 °                      |
| $\omega$                                  | -0.00657141 °                  |
| Inclination                               | 1.67824 °                      |
| $\Omega$                                  | 245.165 °                      |
| Heliocentric velocity at departure (km/s) | (2.45241, -1.13498, 0.0791754) |
| Heliocentric velocity at arrival (km/s)   | (4.80202, -5.12288, 0.190725)  |

Table 3.2.10: Results computed for case 5

### 3.2.6 Case 6: Mars to Earth

|                |                          |
|----------------|--------------------------|
| Departure date | 2033 Jan 18              |
| Arrival date   | 2033 Aug 28              |
| $\Delta t$     | 222 days                 |
| $r_1$          | (1.5831, 0.3913, 0.0306) |
| $r_2$          | (0.9123, 0.4340, 0.0000) |

Table 3.2.11: Data provided for case 6

|   |                                |
|---|--------------------------------|
| Semimajor axis                            | 1.31867                        |
| Eccentricity                              | 0.236873                       |
| $\theta_0$                                | 180 °                          |
| $\omega$                                  | 371.607 °                      |
| Inclination                               | 5.3505 °                       |
| $\Omega$                                  | 205.441 °                      |
| Heliocentric velocity at departure (km/s) | (-6.43846, 8.513846, -0.97904) |
| Heliocentric velocity at arrival (km/s)   | (32.4436, -28.4563, 3.71199)   |

Table 3.2.12: Results computed for case 6



**3.2.7 Case 7: Mars to Earth**

|                |                          |
|----------------|--------------------------|
| Departure date | 2030 Nov 20              |
| Arrival date   | 2031 Jul 06              |
| $\Delta t$     | 228 days                 |
| $r_1$          | (1.4166, 0.8722, 0.0530) |
| $r_2$          | (0.2345, 0.9893, 0.0001) |

Table 3.2.13: Data provided for case 7

|   |                                   |
|---|-----------------------------------|
| Semimajor axis                            | 1.30864                           |
| Eccentricity                              | 0.271869                          |
| $\theta_0$                                | 180 °                             |
| $\omega$                                  | 405.199 °                         |
| Inclination                               | 2.57215 °                         |
| $\Omega$                                  | 256.79 °                          |
| Heliocentric velocity at departure (km/s) | (-9.20594, -5.75652, -0.343519)   |
| Heliocentric velocity at arrival (km/s)   | (0.111769, 0.4865, -0.000106258 ) |

Table 3.2.14: Results computed for case 7

**3.2.8 Case 8: Earth to Mars (hyperbolic)**

|                |                             |
|----------------|-----------------------------|
| Departure date | 2021 Nov 26                 |
| Arrival date   | 2022 Feb 19                 |
| $\Delta t$     | 85 days                     |
| $r_1$          | (0.4383, 0.8843, 0.0000)    |
| $r_2$          | (-0.2082, -1.4582, -0.0255) |

Table 3.2.15: Data provided for case 8

|   |                                   |
|---|-----------------------------------|
| Semimajor axis                            | 1.34023                           |
| Eccentricity                              | 1.44255                           |
| $\theta_0$                                | 288.925 °                         |
| $\omega$                                  | 251.075 °                         |
| Inclination                               | 3.16587 °                         |
| $\Omega$                                  | 243.635 °                         |
| Heliocentric velocity at departure (km/s) | (0.322509, 0.650683, 0 )          |
| Heliocentric velocity at arrival (km/s)   | (-1.20802, -1.22481, -0.0297817 ) |

Table 3.2.16: Results computed for case 8

### 3.2.9 Case 9: Earth to Mars (hyperbolic)

|                |                            |
|----------------|----------------------------|
| Departure date | 2022 Jan 15                |
| Arrival date   | 2022 Apr 20                |
| $\Delta t$     | 95 days                    |
| $r_1$          | (-0.4079, 0.8950, 0.0000)  |
| $r_2$          | (0.6393, -1.2542, -0.0420) |

Table 3.2.17: Data provided for case 9

|   |                                  |
|---|----------------------------------|
| Semimajor axis                            | 5.10169                          |
| Eccentricity                              | 1.11068                          |
| $\theta_0$                                | 280.991 °                        |
| $\omega$                                  | 259.009 °                        |
| Inclination                               | 34.288 °                         |
| $\Omega$                                  | 294.501 °                        |
| Heliocentric velocity at departure (km/s) | (-16.804 , -7.65848 , -12.5916 ) |
| Heliocentric velocity at arrival (km/s)   | (36.9836 , 14.0711 , 26.9253 )   |

Table 3.2.18: Results computed for case 9

## 4 | Conclusions

## 5 | Bibliography

- [1] J. Calaf, "Trajectòries interplanetàries: Patched Conic Approximation," 2017.
- [2] —, "Treballs de Mecànica Orbital," 2017.
- [3] A. Fallis, "Orbital Mechanics for Engineering Students," *Journal of Chemical Information and Modeling*, vol. 53, no. 9, pp. 1689–1699, 2013. [Online]. Available: [https://edisciplinas.usp.br/pluginfile.php/66104/mod{\\_\\_}resource/content/1/OrbitalMechanicsForEngineeringStudents-AerospaceEngineering.pdf](https://edisciplinas.usp.br/pluginfile.php/66104/mod{__}resource/content/1/OrbitalMechanicsForEngineeringStudents-AerospaceEngineering.pdf)
- [4] J. Calaf, "Trajectòries interplanetàries," 2017.